Dynamics of fast pattern formation in porous silicon by laser interference

Ramón J. Peláez, Timo Kuhn, Fidel Vega, and Carmen N. Afonso

Citation: Applied Physics Letters **105**, 161911 (2014); doi: 10.1063/1.4900431
View online: http://dx.doi.org/10.1063/1.4900431
View Table of Contents: http://scitation.aip.org/content/aip/journal/apl/105/16?ver=pdfcov
Published by the AIP Publishing

Dynamics of fast pattern formation in porous silicon by laser interference

Ramón J. Peláez,[1] Timo Kuhn,[1] Fidel Vega,[2] and Carmen N. Afonso[1]
[1]*Laser Processing Group, Instituto de Óptica, CSIC, Serrano 121, 28006 Madrid, Spain*
[2]*Departament d'Òptica i Optometria, UPC, Violinista Vellsolà 37, 08222 Terrasa, Spain*

(Received 3 September 2014; accepted 14 October 2014; published online 24 October 2014)

Patterns are fabricated on 290 nm thick nanostructured porous silicon layers by phase-mask laser interference using single pulses of an excimer laser (193 nm, 20 ns pulse duration). The dynamics of pattern formation is studied by measuring in real time the intensity of the diffraction orders 0 and 1 at 633 nm. The results show that a transient pattern is formed upon melting at intensity maxima sites within a time <30 ns leading to a permanent pattern in a time <100 ns upon solidification at these sites. This fast process is compared to the longer one (>1 μs) upon melting induced by homogeneous beam exposure and related to the different scenario for releasing the heat from hot regions. The diffraction efficiency of the pattern is finally controlled by a combination of laser fluence and initial thickness of the nanostructured porous silicon layer and the present results open perspectives on heat release management upon laser exposure as well as have potential for alternative routes for switching applications. © *2014 AIP Publishing LLC*.
[http://dx.doi.org/10.1063/1.4900431]

Nanostructured porous silicon (nanoPS) is a nanocrystalline material with a large internal surface[1] that makes it very attractive for sensing and biomedical applications.[2,3] Patterned structures on nanoPS have recently been proposed for diffraction-based biosensors[4,5] or as platforms for drug delivery[6] or cell adhesion.[7,8] Additionally, surface microstructure can substantially enlarge cell alignment and culture.[7,9] Patterns have been fabricated in nanoPS through mask-based processes like ion beam irradiation,[8] anisotropic chemical wet etching followed by porosification,[10] dry soft lithography,[11] stamp pressing,[4] or laser writing.[12,13] However, none of these methods has the capability to offer flexibility in the pattern design over large areas in a time-efficient and single-step process. Laser interference has instead recently been demonstrated[14] as a single-step and versatile method for producing tailored diffraction-based platforms in nanoPS over areas of a few mm^2 on which human mesenchymal stem cells have directly bound and aligned.[7]

Although laser interference has been applied in the 1990s to produce periodic structures in nanoPS[15] these works were focused to morphological aspects rather than to structural ones and little is known on the dynamics or underlying mechanism of the process. Furthermore, the studies on the interaction of laser pulses with nanoPS have almost exclusively been focused to report its lower melting threshold with respect to crystalline c-Si.[16,17] In order to fully exploit the capabilities of laser interference for patterning nanoPS for bioassays, there is a need for understanding the underlying mechanisms that eventually allow controlling the transformed material properties and pattern features. Furthermore, there are no reports on whether the transformation dynamics upon laser interference (modulated beam) or homogeneous beam exposure is the same or the alternation of cold and hot regions in the pattern makes any difference. In this letter, we aim to provide direct evidence that formation of patterns by laser interference with a single ns pulse is much faster than the process upon homogeneous beam exposure and that the diffractive properties can be controlled through the laser fluence and layer thickness.

The nanoPS layers were fabricated following the standard procedure using an etching current of 80 mA cm^{-2}. The porosity of the layers has been determined by measuring the spectral reflectance. A good fit to the experimental data was achieved for a first 6 nm layer of low porosity (55%) on top of the c-Si substrate, followed by an intermediate 23 nm thick layer (63% porosity) and a top 261 nm thick layer (79% porosity). Altogether, the nanoPS sample studied in this work has a thickness of 290 nm. Further details can be found elsewhere.[7,14]

The nanoPS sample was patterned using an excimer laser (193 nm, 20 ns) pulses to expose a fringed phase mask. With the selected projection optics, the sample is finally exposed to an intensity modulated by maxima and minima of interference with a period $\Delta = 6.3\,\mu$m.[7,14,18] The fluence at the sample site is thus modulated along the direction perpendicular to the fringes ($\boldsymbol{x}$ axis) as $F(x) = \boldsymbol{F}\,(1 + \cos(2\pi x/\Delta))$, where $\boldsymbol{F}$ is the average fluence experimentally measured at the sample site. The fluence is thus modulated between 0 and $\boldsymbol{2F}$ across the pattern. $\boldsymbol{F}$ and $\boldsymbol{2F}$ will be referred to from now on as fluence and peak fluence, respectively.

Figure 1(a) shows an optical image of the edge of a pattern produced at the highest fluence and taken with an optical Microscope Eclipse Ti operating in reflexion configuration at $\lambda = 455$ nm. From left to right, grey fringes are seen that increase their width until their contrast covers the whole sample. These fringes have the same contrast than the as-grown material and must thus correspond to the regions of the pattern that are non-transformed, i.e., exposed to the intensity minima. The other areas show the inverse behaviour, i.e., their width decreases until they are no longer visible and should thus be the ones exposed to the intensity maxima. In addition, while their contrast is darker than that of the as grown material for very low fluences (right side of the image), it becomes first brighter and later complex (a dark center surrounded by bright areas) as we move to the left of the image, i.e., increasing fluence. When exposed to a He-Ne probe beam ($\lambda = 633$ nm), a diffraction pattern is observed in

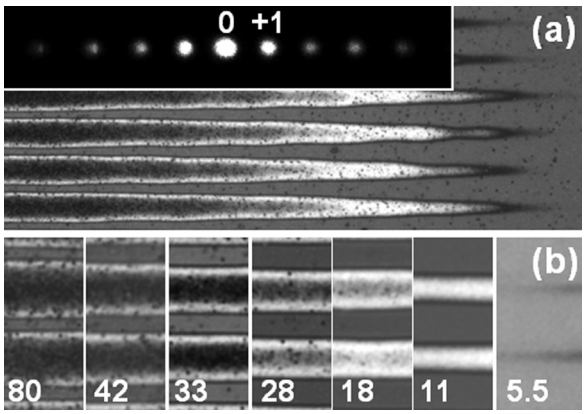

FIG. 1. (a) Optical image of the edge of a pattern produced upon modulated beam exposure with fluence of 80 mJ cm^{-2}; the inset shows the diffraction pattern where the labels refer to the diffraction orders recorded in this work. (b) Optical images of center of patterns produced at decreasing fluences from left to right; the labels are the fluence values in mJ cm^{-2}.

reflection (Fig. 1(a)). It is consistent with the Fourier transform of the optical image, its one-dimensional character and period ($\Delta = 6.3\ \mu m$).

A more quantitative evolution of the pattern features with fluence is seen in Fig. 1(b), where two transformed regions of the central part of patterns produced with different fluences are shown, evidencing that the width of transformed regions varies little for fluences >18 mJ cm^{-2}. In addition, the pattern produced at 5.5 mJ cm^{-2} (or at a peak fluence of 11 mJ cm^{-2}) must be very close to the threshold fluence for pattern formation since the dark lines (as seen in Fig. 1(b)) for this fluence are barely discernible and discontinuous along the patterned area. This value is in quite good agreement with the melting threshold of 15 ± 2 mJ cm^{-2} reported elsewhere upon homogeneous beam exposure.[16,17]

The probe beam is also used to record in real time the intensity of the 0 and 1 diffracted beams in reflection mode that will be referred to from now on as real-time reflectivity (RTR) transients. This type of measurements have since very long been applied to record the specular reflectivity in order to understand the dynamics of a large variety of laser induced processes in semiconductors.[19–21] When applied to nanoPS,[16,17] the transient features were consistent with surface melting, the presence of intensive hydrogen evaporation and ablation of the nanoPS surface. However, there are no reports on the use of RTR measurements to study the dynamics of pattern formation either in nanoPS or other materials.

The probe beam is pulsed to 1 μs by means of an acousto-optic modulator and then focused at the center of the irradiated area at ≈33° off its normal. It is synchronized with the irradiation laser pulse to record simultaneously the intensity of the orders 1 (D) and 0 (R) of the diffracted beam (as labeled in Fig. 1(a)) as a function of time with a two-channel fast oscilloscope.[19,20] Transients recorded in the diffraction orders 1 and 0 are, respectively, shown in Figs. 2(a) and 2(b). The origin of the x-axis is set at the time the excimer laser pulse reaches its maximum. It is seen that a minimum fluence of 11 mJ cm^{-2} is necessary to record any intensity in the diffraction order 1 as well as to induce a surface pattern formation consistently with the optical images shown in Fig. 1(b). For higher fluences, the transients of both orders exhibit approximately the same but inverse behavior, i.e., the intensity increases/decreases very rapidly from the initial level ($0/R_i$) to a maximum/minimum value (D_m/R_m) for the orders 1 and 0, respectively. As time progresses, the intensity decreases/ increases to a final value (D_f/R_f) that is always higher/lower than the initial levels $0/R_i$. All R values (R_f and R_m) are referred to the initial values as $(R - R_i)/R_i$.

To help in understanding these transient changes, we have also irradiated the nanoPS layer using a homogenizer to expose homogenously areas of $\approx 4 \times 4\ mm^2$ that will be referred to from now on as homogeneous beam exposure. The transients are shown in Fig. 2(c) and have similar features to those plot in Fig. 2(b) for order 0 as expected with a couple of exceptions: the minimum at R_m is less pronounced and occurs at longer times, and above all, the whole process is not completed in the time scale chosen. A time >1 μs is needed to achieve the constant R_f levels that are indicated on the right hand side of Fig. 2(c) as horizontal lines.

In an earlier work,[14] we have shown that exposure to a modulated beam intensity leads to local heterogeneous melting in the regions exposed to the laser intensity maxima and the formation of Si nanoparticles (NPs) upon solidification. Same type of NPs are observed in the whole area exposed to the homogeneous beam and this result is in agreement with previous work[16] in which similar NPs were found following melting and solidification of much thicker nanoPS layers.

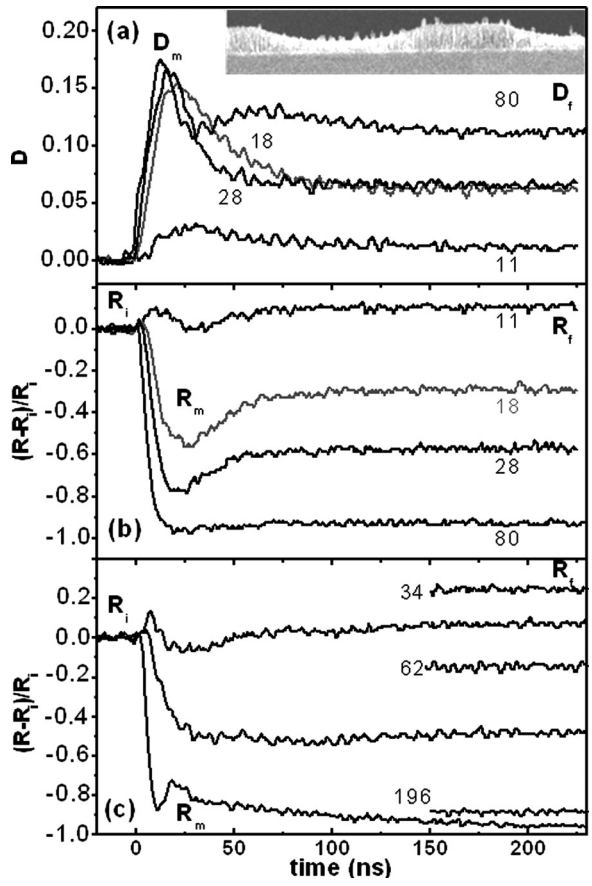

FIG. 2. RTR transients recorded upon modulated beam intensity in the (a) order 1 and (b) order 0, and (c) upon homogeneous beam exposure. The labels are the fluence values in mJ cm^{-2}. The inset shows a cross section scanning electron microscopy image recorded in the sample irradiated with a fluence of 28 mJ cm^{-2} and taken from Ref. 14.

The melting process and the NPs formation occur at the expense of reducing the thickness of the nanoPS layer; the higher the fluence, the higher the thickness decrease.[14] As a consequence, the resulting diffractive pattern consists of alternate hills and trenches, the latter being covered by Si NPs as shown in the inset in Fig. 2(a).

Figure 3 shows several parameters extracted from RTR transients as a function of peak fluence, in order to ease the comparison of results upon modulated and homogeneous beam exposures. Upon modulated beam intensity (Figs. 3(a) and 3(b)), D_m/R_m and D_f/R_f increase/decrease with fluence and for peak fluences higher than ≈80 mJ cm^{-2}, both R and D keep changing but at a much lower rate. This is consistent with earlier work[14] showing that the closer the trench depth is to the nanoPS thickness (or nanoPS/c-Si interface), the higher the fluence required for reaching the melting temperature due to the lower porosity. It is worth mentioning that the melting temperature of our nanoPS with 79% porosity was found to be 1198 K,[14] i.e., significantly smaller than that of c-Si (1685 K), and consistent with the value and the decrease of melting temperature with porosity reported in Ref. 17. The same trend, sign of changes and values are observed for R_m upon homogeneous beam intensity (Fig. 3(b)). A monotonous decrease is instead observed for R_f and the values are generally higher upon homogeneous than modulated beam intensity. The reason for these differences in R_f can be twofold. On the one hand, once the diffraction efficiency of the patterns becomes relevant and thus, there is significant signal in the order 1, the intensity in order 0 becomes distributed among the several orders of diffraction. On the other hand, the refractive index of the sample upon modulated beam exposure is inhomogeneous since the sample has alternate regions of Si NPs and nanoPS, while the whole sample is covered by NPs upon homogeneous beam intensity.

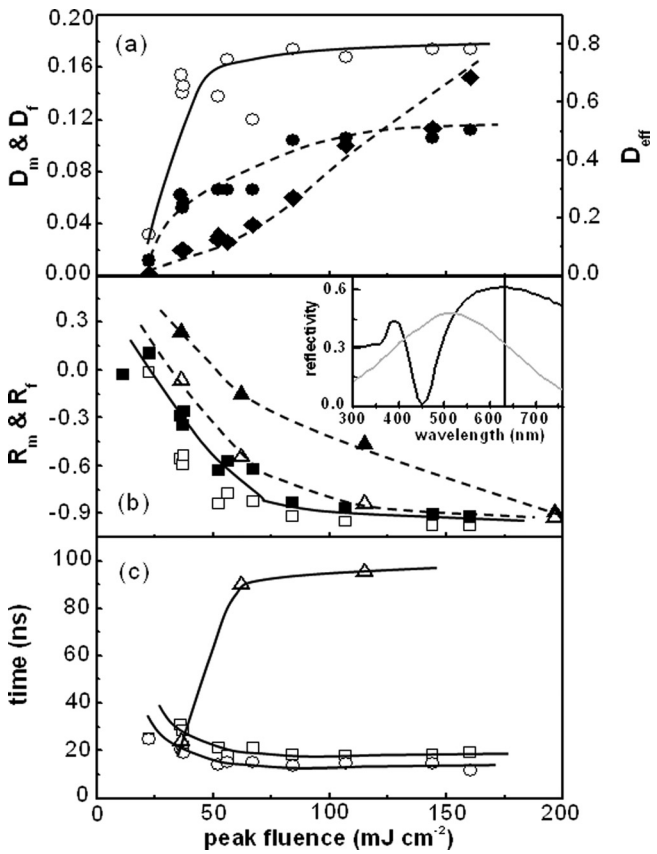

FIG. 3. Parameters extracted from the RTR transients recorded upon modulated and homogeneous beam intensity as a function of peak fluence: (a) (●) D_f and (○) D_m values for order 1 and (◆) D_{eff} calculated from diffraction patterns such as that in the inset of Fig. 1(a); (b) (■) R_f and (□) R_m values for order 0 and (▲) R_f and (Δ) R_m values for homogeneous beam; (c) time to reach (□) R_m in order 0 and (Δ) homogeneous beam exposure, and (○) D_m in order 1 after the laser maximum. All lines are guidelines. The inset in Fig. 3(b) shows the reflectivity spectra measured (black line) before and (grey line) after irradiation with a homogeneous beam at 115 mJ cm^{-2} and the vertical line marks the wavelength (633 nm) of the probe beam.

The diffraction efficiency (D_{eff}) of patterns is determined by the ratio of the integrated intensities of the diffraction orders 1 and 0 (from inset in Fig. 1(a)) and plotted in Fig. 3(a) as a function of peak fluence. Same trend is achieved from the RTR transients by calculating D_{eff} as the final intensity of the signal in order 1 (D) to 0 (R) ratio. The observed increase of D_{eff} as fluence increases is consistent with the increase of the depth of the trenches reported elsewhere[14] thus evidencing that the final diffractive properties relate to topography.

If surface melting were the only process occurring at the early stages of the irradiation process, the presence of liquid Si should induce a sharp increase of the reflectivity at the probe beam wavelength.[17,19,20] Instead, the transients obtained at peak fluences ≥18 mJ cm^{-2} upon modulated (0 order, Fig. 2(b)) and homogeneous (Fig. 2(c)) beam exposures show a fast intensity decrease. While this fast initial change must undoubtedly relate to surface melting, the sign of the change (decrease) relates to the modification of the thickness of the nanoPS layer at intensity maxima sites. To illustrate this interpretation, we have included as an inset in Fig. 3(b), the reflectivity spectra measured at s polarization before and after irradiation. The spectrum of the as-grown material exhibits interferential effects with maxima and minima of reflectivity due to multiple reflections at the layer interfaces. Upon irradiation, the thickness of the nanoPS layer is reduced thus leading to a blue shift of the maxima and minima, and eventually resulting in a significantly lower reflectivity at the probe beam wavelength. The earlier reported reflectivity increase[17] is thus most likely related on the one hand to the much larger thickness of the nanoPS layer (5–7 μm) that together with surface roughness might prevent interference effects within the layer. On the other hand, the penetration depth of the irradiation laser that is much higher due to its longer wavelength: 107–302 nm at 308 nm in Ref. 17 for porosities of 75%–82% and 39 nm at 193 nm in this work for 79% porosity. The higher penetration depth induces a thicker molten layer of Si on top of the nanoPS leading to the reflectivity being insensitive to any thickness reduction of the nanoPs layer. All together allows us concluding that the sign of the intensity changes (both transient and final values) as well as the diffractive properties of patterns are controlled by a combination of laser fluence and nanoPS layer thickness, the latter parameter limiting the highest accessible diffraction efficiency.

The transients recorded at the threshold fluence to observe permanent changes show different features that provide further support to the above reasoning. Upon homogeneous beam exposure (Fig. 2(c)), the transient recorded at

34 mJ cm^{-2} shows a fast reflectivity increase followed by a minimum and a rise to a final value R_f higher than the initial one. At such low fluence, there is a very shallow heterogeneous surface melting with negligible reduction of the layer thickness and formation of Si NPs occurs on top of the large remnant nanoPS layer upon cooling and solidification.[14] Hence, in absence of significant thickness reduction, the formation of Si NPs leads to the observed higher R_f compared to the initial one. Similar changes are observed in the transients obtained in the orders 1 and 0 (Figs. 2(a) and 2(b)) around threshold (11 mJ cm^{-2}). These changes are thus consistent with the formation of a transient pattern formed by alternate very shallow heterogeneously molten Si (regions exposed to the intensity maxima) and regions of non-transformed nanoPS (regions exposed to the intensity minima), with negligible reduction of layer thickness. This interpretation is consistent with the very low D_f and D_{eff} values achieved for this fluence supporting further that D_{eff} is mainly related to pattern topography.

Overall, the most distinct feature between modulated and homogeneous exposure is the time scale of the processes as shown in Fig. 3(c). Upon modulated beam exposure, the time required to melt at intensity maxima (i.e., to reach R_m/D_m) is always very short (<30 ns), decreases with fluence and reaches a saturation value <15 ns for order 1. Upon homogeneous beam exposure, this time increases with fluence and reaches a large saturation value of the order of 100 ns. This process leads to a fast and significant intensity transient signal at the position of order 1 that could have a potential for switching applications.

A good approximation for the solidification process is the time needed to achieve R_f since the variation of the optical constants of Si with temperature up to the melting temperature is at the most 19%.[19] While this time is <100 ns upon modulated beam exposure, it becomes >1 μs upon homogeneous beam exposures. This comparison allows us to conclude that the cooling process is much faster upon modulated beam exposure and the explanation has to relate to the different thermal scenario for releasing the heat from hot regions. Upon homogeneous beam exposure, the surface molten layer can only cool down through heat flow along the in-depth direction while upon modulated beam exposure, there are alternate hot and colder regions which offer paths for lateral heat sink. The thermal conductivity of nanoPS is known to depend not only on porosity but also to be smaller across than along the pores. The former is reported to decrease first very sharply with porosity and to become approximately constant for porosities higher than 15% and up to 30%.[22] Using this approximately constant value, the calculated diffusion length (≈200 nm in 100 ns) results small enough as to discard the lateral heat flow influencing the melting process and the transformed regions width for the pattern period studied. It appears instead to be long enough to speed up the cooling process.

In summary, this work shows that laser interference produces a transient pattern formed by liquid Si at intensity maxima sites that leads to a permanent pattern. The regions where melting of nanoPS takes place become covered by Si nanoparticles upon solidification and reduce their effective thickness and thus the patterns have topography of hills and trenches. The melting process is completed within a time shorter than twice the pulse duration and the whole process is completed within <100 ns due to lateral heat flow from molten regions at maximum intensity sites towards colder regions at minima intensity sites. This interpretation is further confirmed by the fact that the melting–solidification process upon homogeneous beam exposure where these extra paths for cooling are missing, lasts >1 μs. The sign of the transient and final reflectivity changes depend on the modification of the thickness of the nanoPS layer and the penetration depths of the irradiation and probe beams. Finally, the diffractive efficiency of the patterns is controlled by a combination of laser fluence and initial nanoPS layer thickness, the latter parameter limiting the highest accessible values.

This work has partially been supported under Project MAT2011-28345-C02-02 (Spain). R. J. Peláez and T. Kuhn acknowledge respectively the Grant JCI-2012_13034 from the Juan de la Cierva program and the support of DAAD. The authors gratefully thank Professor P. Leiderer from University of Konstanz for his support and Dr. G. Recio from Universidad Autónoma de Madrid for the sample.

[1]V. Lehmann, *Electrochemistry of Silicon* (Wiley-VCH, Weinheim, 2002).
[2]R. J. Martín-Palma, M. Manso-Silván, and V. Torres-Costa, J. Nanophotonics **4**, 042502 (2010).
[3]A. Angelescu, I. Kleps, M. Mihaela, M. Simion, T. Neghina, S. Petrescu, N. Moldovan, C. Paduraru, and A. Raducanu, Rev. Adv. Mater. Sci. **5**, 440 (2003).
[4]J. D. Ryckman, M. Liscidini, J. E. Sipe, and S. M. Weiss, Appl. Phys. Lett. **96**, 171103 (2010).
[5]M. Liscidini and J. E. Sipe, Appl. Phys. Lett. **91**, 253125 (2007).
[6]E. J. Anglin, L. Cheng, W. R. Freeman, and M. J. Sailor, Adv. Drug Delivery Rev. **60**, 1266 (2008).
[7]R.-J. Peláez, C.-N. Afonso, F. Vega, G. Recio-Sánchez, V. Torres-Costa, M. Manso-Silván, J.-P. García-Ruiz, and R.-J. Martín-Palma, J. Biomed. Mater. Res. Part B **101B**, 1463 (2013).
[8]V. Torres-Costa, G. Martínez-Muñoz, V. Sánchez-Vaquero, A. Muñoz-Noval, L. González-Méndez, E. Punzón-Quijorna, D. Gallach-Pérez, M. Manso-Silván, A. Climent-Font, J. P. Gracía-Ruiz, and R. J. Martín-Palma, Int. J. Nanomed. **7**, 623 (2012).
[9]M. Hoffmann, J. P. Kuska, M. Zscharnack, M. Loeffler, and J. Galle, PLoS One **6**, e21960 (2011).
[10]I. Kleps, M. Miu, M. Simion, T. Ignat, A. Bragaru, F. Craciunoiu, and M. Danila, J. Biomed. Nanotechnol. **5**, 300 (2009).
[11]D. J. Sirbuly, G. M. Lowman, B. Scott, G. D. Stucky, and S. K. Burrato, Adv. Mater. **15**, 149 (2003).
[12]Y.-L. Khung, S. D. Graney, and N. H. Voelcker, Biotechnol. Progr. **22**, 1388–1393 (2006).
[13]L. De Stefano, I. Rea, M. Arcangela Nigro, F. G. Della Corte, and I. Rendina, J. Phys.: Condens. Matter **20**, 265009 (2008).
[14]F. Vega, R. J. Peláez, T. Kuhn, C. N. Afonso, G. Recio-Sánchez, and R. J. Martín-Palma, J. Appl. Phys. **115**, 184902 (2014).
[15]V. I. Vlad, A. Petris, V. N. Chumash, and I. Cojocaru, Appl. Surf. Sci. **106**, 356 (1996).
[16]T. Dittrich, I. Sieber, W. Henrion, S. Rauseher, N. Wanderka, and J. Rappich, Appl. Phys. A **63**, 467 (1996).
[17]V. Y. Timoshenko, T. Dittrich, I. Sieber, J. Rappich, B. V. Kamenev, and P. K. Kashkarov, Phys. Status Solidi **182**, 325 (2000).
[18]J. Huster, J. Müller, H. Renner, and E. Brinkmeyer, J. Lightwave Technol. **29**, 2621 (2011).
[19]G. E. Jellison, Jr., D. H. Lowndes, D. N. Mashburn, and R. F. Wood, Phys. Rev. B **34**, 2407 (1986).
[20]J. Solis and C. N. Afonso, J. Appl. Phys. **69**, 2105 (1991).
[21]F. Vega, R. Serna, C. N. Afonso, D. Bermejo, and G. Tejeda, J. Appl. Phys.**75**, 7287 (1994).
[22]J. D. Chung, KSME Int. J. **13**, 762 (1999).